



# Multifunctional superparamagnetic nanocarriers with folate-mediated and pH-responsive targeting properties for anticancer drug delivery

Miao Guo<sup>a</sup>, Chailu Que<sup>a</sup>, Chenhong Wang<sup>b</sup>, Xiaozhou Liu<sup>a</sup>, Husheng Yan<sup>a,\*</sup>, Kelian Liu<sup>b,\*\*</sup>

<sup>a</sup> Key Laboratory of Functional Polymer Materials, Ministry of Education; and Institute of Polymer Chemistry, Nankai University, Tianjin 300071, China

<sup>b</sup> Beijing Institute of Pharmacology and Toxicology, Beijing 100850, China

## ARTICLE INFO

### Article history:

Received 23 July 2010

Accepted 14 September 2010

Available online 9 November 2010

### Keywords:

Drug delivery

Magnetism

Nanoparticle

Nanocarrier

pH-responsive

Folate-mediated targeting

## ABSTRACT

Multifunctional nanocarriers with multilayer core-shell architecture were prepared by coating superparamagnetic Fe<sub>3</sub>O<sub>4</sub> nanoparticle cores with a mixture of the triblock copolymer methoxy poly(ethylene glycol)-*b*-poly(methacrylic acid-*co*-*n*-butyl methacrylate)-*b*-poly(glycerol monomethacrylate) and the folate-conjugated block copolymer folate-poly(ethylene glycol)-*b*-poly(glycerol monomethacrylate). The model anticancer agent adriamycin (ADR), containing an amine group and a hydrophobic moiety, was loaded into the nanocarrier at pH 7.4 by ionic bonding and hydrophobic interactions. The release rate of the loaded drug molecules was slow at pH 7.4 (i.e. mimicking the blood environment) but increased significantly at acidic pH (i.e. mimicking endosome/lysosome conditions). Acid-triggered drug release resulted from the polycarboxylate protonation of poly(methacrylic acid), which broke the ionic bond between the carrier and ADR. Cellular uptake by folate receptor-overexpressing HeLa cells of the folate-conjugated ADR-loaded nanoparticles was higher than that of non-folate-conjugated nanoparticles. Thus, folate conjugation significantly increased nanoparticle cytotoxicity. These findings show the potential viability of a folate-targeting, pH-responsive nanocarrier for amine-containing anticancer drugs.

© 2010 Elsevier Ltd. All rights reserved.

## 1. Introduction

A major challenge to successful cancer chemotherapy is achieving specific drug accumulation at the tumor sites. Most of the available anticancer agents cannot distinguish between cancerous and healthy cells, leading to systemic toxicity and undesired side effects. Solutions to this problem have focused on the development of nanoscale tumor-targeted delivery systems. Various nanocarriers including liposomes, polymeric nanoparticles, block copolymer micelles, and dendrimers have been developed for the targeted delivery of therapeutics to cancerous tissues [1–5]. Nanocarriers are also used to deliver imaging agents (e.g. superparamagnetic iron oxide nanoparticles as magnetic resonance imaging (MRI) contrast agent) for diagnostics and real-time particle tracking in the body. Long-circulating nanocarriers such as poly(ethylene glycol) (PEG)- and poly(ethylene oxide) (PEO)-modified nanocarrier systems can preferentially accumulate in the tumor sites through the leaky tumor neovasculature by the enhanced permeability and retention (EPR) effect, known as the passive targeting [6,7].

To further improve delivery efficiency and cancer specificity, active targeting strategies are currently under wide investigation. One of the most common such strategies involves coupling the nanocarrier surface with a specific ligand that is recognizable by cells present at the disease site [8]. Various specific receptors (e.g. vitamins and sugar receptors) overexpressed on the cancer cell surface have served as useful targets. Folate receptors are selectively overexpressed on brain, kidney, lung, and breast cancer cells. Folate (vitamin M) has a low molecular weight and a high receptor affinity ( $K_d = 1 \times 10^{-10}$  M) [9,10]. Nanocarriers conjugated with folate can be targeted to and internalized into target cells through receptor-mediated endocytosis [11–14].

Another promising targeting approach is the use of stimuli-responsive delivery systems that are sensitive to changes in biological and environmental signals such as pH, temperature, and specific enzymes [15–17]. Ideal drug delivery systems should be stable with a long circulation time, and should keep the loaded drugs unreleased during circulation in the bloodstream or in normal tissues. Upon reaching and accumulating in tumor tissues by passive and active targeting, and after being taken up by cancer cells, the systems should release the drugs rapidly in response to the local environment.

Smart drug delivery systems have been developed in which the drug is loaded by acidic pH-induced cleavable covalent bonds. For

\* Corresponding author. Fax: +86 22 2350 3510.

\*\* Corresponding author. Fax: +86 10 6821 1656.

E-mail addresses: [yanhs@nankai.edu.cn](mailto:yanhs@nankai.edu.cn) (H. Yan), [keliangliu@yahoo.com](mailto:keliangliu@yahoo.com) (K. Liu).

example, adriamycin (ADR) can be attached to the side chain of a core-forming segment by an acid-labile hydrazone bond. This bond is stable at physiological pH (7.0–7.4) but degraded at the lower pH of endosomal/lysosomal compartments (pH 5.0–5.5) [18,19]. Drugs may otherwise be loaded into the core of polymeric micelles by non-covalent interactions, in most cases, hydrophobic [20,21], or ionic interactions [22,23]. Recently, our group successfully loaded drugs with ionizable groups and hydrophobic moieties into nanocarriers by the combined action of ionic bonding and hydrophobic interactions [24,25]. The use of non-covalent interactions resulted in a high loading affinity at a neutral pH (7.4), preventing premature release into the bloodstream. The loaded drugs released with good kinetics at an acidic pH, which breaks the ionic bonding.

In this paper, we report the development of multifunctional nanocarriers with a superparamagnetic  $\text{Fe}_3\text{O}_4$  core, carboxyl-containing inner shell with adjustable hydrophobicity, biocompatible PEG outermost shell, and a small amount of surface-conjugated folate. The multifunctional nanocarriers were prepared by coating a superparamagnetic  $\text{Fe}_3\text{O}_4$  core with a mixture of the triblock copolymer methoxy poly(ethylene glycol)-*b*-poly(methacrylic acid-*co*-*n*-butyl methacrylate)-*b*-poly(glycerol monomethacrylate) (denoted MPEG-*b*-P(MAA-*co*-*n*BMA)-*b*-PGMA) and the folate-conjugated block copolymer folate-poly(ethylene glycol)-*b*-poly(glycerol monomethacrylate) (denoted FA-PEG-*b*-PGMA) (Scheme 1). As a model drug with an amine group and a hydrophobic moiety, ADR was loaded into the nanocarrier at pH 7.4 by ionic bonding and hydrophobic interactions. The nanocarrier possessed a superparamagnetic  $\text{Fe}_3\text{O}_4$  nanoparticle core, which may serve as MRI contrast agent and hyperthermic agent, folate conjugation on the surface, which was recognized by HeLa cells, and property of pH-responsive release of the loaded drug.

## 2. Experimental

### 2.1. Materials

Methoxy poly(ethylene glycol) (MPEG-OH, 2000 Da, Aldrich) and poly(ethylene glycol) (HO-PEG-OH, 3000 Da, Fluka) were dehydrated by azeotropic distillation of water in toluene, precipitated with cold ethyl ether, filtered, washed with ether, and vacuum-dried. *tert*-Butyl methacrylate (*t*BMA, Acros) and *normal*-butyl methacrylate (*n*BMA, Acros) were distilled over  $\text{CaH}_2$  under reduced pressure before use. 1,1,4,7,7-Pentamethyldiethylenetriamine (PMDETA) was purchased from Acros. 2-Bromoisobutyl bromide (BIBB) was purchased from Aldrich. Folate (FA) was purchased from Tianjin Guangfu Fine Chemical Research Institute. Solketal methacrylate (SMA) was prepared by reaction of solketal

(2,2-dimethyl-1,3-dioxane-4-methanol) with methacryloyl chloride, according to our previous reports [26,27]. Adriamycin hydrochloride (ADR·HCl) was purchased from Shenzhen Main Luck Pharmaceuticals Inc. (Shenzhen, China). The human cervical carcinoma HeLa cell line was obtained from the Cell Resource Center of Peking Union Medical College. RPMI 1640, RPMI 1640 without folic acid, RPMI 1640 without phenol red, and fetal bovine serum (FBS) were purchased from GIBCO (Uxbridge, UK).

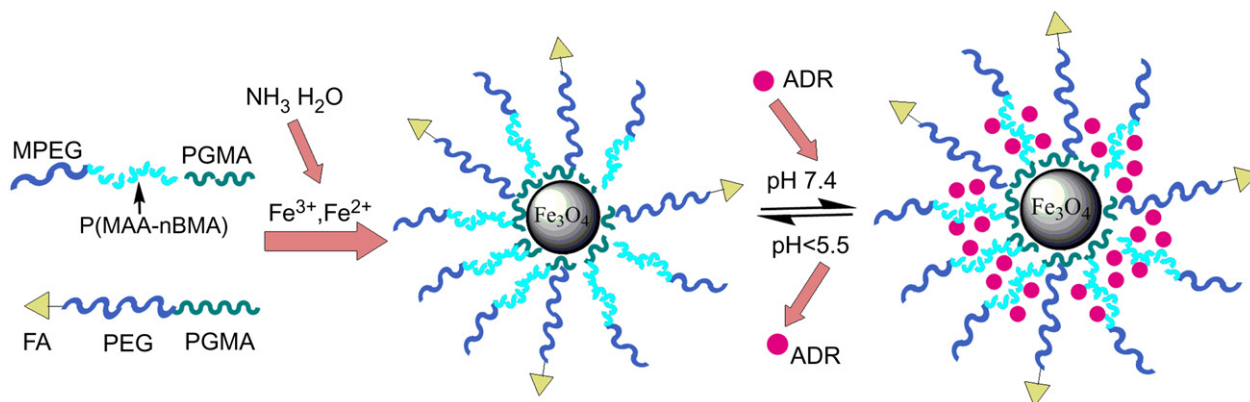
### 2.2. Block copolymer synthesis

The triblock copolymer MPEG-*b*-PMAA-*b*-PGMA was synthesized by atom transfer radical polymerization (ATRP) as reported previously [24]. The block copolymer MPEG-*b*-P(MAA-*co*-*n*BMA)-*b*-PGMA was similarly synthesized, except that a mixture of *t*BMA and *n*BMA was used instead of *t*BMA alone. Molar ratios ([*t*BMA]:[*n*BMA]) of 9:1 and 8:2 yielded MPEG-*b*-P(MAA<sub>19</sub>-*co*-*n*BMA<sub>4</sub>)-*b*-PGMA<sub>25</sub> and MPEG-*b*-P(MAA<sub>17</sub>-*co*-*n*BMA<sub>10</sub>)-*b*-PGMA<sub>17</sub>, respectively.

The macroinitiator OH-PEG-Br was synthesized by reacting OH-PEG-OH with 2-bromoisobutyl bromide (1:1 M ratio), using a similar process as one reported previously [27]. Folic acid (1.5 mmol) dissolved in 10 mL dimethyl sulfoxide (DMSO) was preactivated with *N,N'*-diisopropylcarbodiimide (DIC, 1.5 mmol) at room temperature for 4 h. Dehydrated OH-PEG-Br (1 mmol) and 4-dimethylamino pyridine (catalyst, 0.1 mmol) were dissolved in 10 mL of DMSO. Preactivated folic acid was added dropwise to the solution, and the mixture was stirred at 50 °C for 12 h. A light yellow powder, FA-PEG-Br, was obtained after precipitation with cold ethyl ether, recrystallized three times to remove unreacted folate, and vacuum-dried. The diblock copolymer folate-PEG-*b*-PGMA was synthesized using FA-PEG-Br as a macroinitiator by a procedure similar to one reported previously [26,27]. The structure and polydispersity index of all the synthesized copolymers were measured (Table 1).

### 2.3. Preparation of copolymer-coated $\text{Fe}_3\text{O}_4$ nanocarriers

$\text{Fe}_3\text{O}_4$  nanoparticles coated with MPEG-*b*-PMAA<sub>18</sub>-*b*-PGMA<sub>15</sub>, MPEG-*b*-P(MAA<sub>19</sub>-*co*-*n*BMA<sub>4</sub>)-*b*-PGMA<sub>25</sub>, or MPEG-*b*-P(MAA<sub>17</sub>-*co*-*n*BMA<sub>10</sub>)-*b*-PGMA<sub>17</sub> were prepared by alkaline coprecipitation of  $\text{Fe}^{2+}/\text{Fe}^{3+}$  (1:2 M ratio) in the presence of the corresponding copolymers in aqueous solution using procedures similar to those reported previously [24,27].  $\text{Fe}_3\text{O}_4$  nanoparticles coated with a mixture of MPEG-*b*-P(MAA<sub>19</sub>-*co*-*n*BMA<sub>4</sub>)-*b*-PGMA<sub>25</sub> and folate-PEG-PGMA<sub>34</sub> (9:1 M ratio) were prepared by the same method. The iron content of the nanocarriers was determined by spectrophotometry at 340 nm



**Scheme 1.** Schematic representation of the preparation of MPEG-*b*-P(MAA-*co*-*n*BMA)-*b*-PGMA/FA-PEG-*b*-PGMA- $\text{Fe}_3\text{O}_4$  nanocarriers and ADR loading and release.

**Table 1**  
Structure of block copolymers.

Copolymer	DR of PMAA segment <sup>a</sup>	DR of PnBMA segment <sup>a</sup>	DR of PGMA segment <sup>a</sup>	PDI <sup>b</sup>
MPEG- <i>b</i> -PMAA <sub>18</sub> - <i>b</i> -PGMA <sub>15</sub>	18	—	15	1.18
MPEG- <i>b</i> -P(MAA <sub>19</sub> - <i>co</i> -nBMA <sub>4</sub> )- <i>b</i> -PGMA <sub>25</sub>	19	4	25	1.15
MPEG- <i>b</i> -P(MAA <sub>17</sub> - <i>co</i> -nBMA <sub>10</sub> )- <i>b</i> -PGMA <sub>17</sub>	17	10	17	1.21
FA-PEG- <i>b</i> -PGMA <sub>34</sub>	—	—	34	—

Molecular weights of MPEG and PEG were 2000 Da and 3000 Da, respectively, as given by the supplier.

<sup>a</sup> The degree of polymerization (DR) of each segment was derived from the DR of the corresponding segment of the precursor polymer, which was determined by <sup>1</sup>H NMR using MPEG or PEG segments as a reference.

<sup>b</sup> Polydispersity index of the precursor polymers determined by GPC.

(TU1810PC UV–vis spectrometer, Beijing Purkinje General Instrument Co.) after a 2-h digestion of the nanoparticles in 30% v/v HCl at elevated temperatures (50–60 °C) as described previously [28].

The average particle size, size distribution, and morphology of the copolymer-coated nanoparticles were studied by transmission electron microscopy (TEM) and dynamic light scattering (DLS). The TEM measurement was performed on a JEM-2010F transmission electron microscopy (JEOL, JAPAN). A drop of well-dispersed nanoparticle dispersion was placed onto an amorphous carbon-coated 200-mesh copper grid, followed by drying the sample at ambient temperature before it was loaded onto the microscope. The DLS analysis and zeta potential measurement of samples dispersed in deionized water was performed on a BI-200SM (Brookhaven, NY, USA) equipped with a BI-900AT digital correlator at 636 nm. Sample magnetization was measured as a function of the applied magnetic field *H* with a 9600VSM (LDJ, USA) superconducting quantum interference device (SQUID) magnetometer. The hysteresis of the magnetization was obtained by changing *H* between +6000 and –6000 Oe at 300 K.

#### 2.4. Drug loading and release

Drug loading was performed as described below. The nanoparticle suspension was dialyzed (MWCO 14,000) against phosphate buffer (pH 7.4) for 12 h, followed by dialysis against water for 1 h. An aqueous solution of ADR·HCl (3 mL, 2 mg/mL) was added dropwise to the dialyzed suspension. After stirring overnight, the suspension was dialyzed (MWCO 14,000) against water, which was changed 10–15 times over 3 d to remove the free ADR. The loading capacity was estimated by subtracting the amount of ADR in the collected outside solution (determined by spectrophotometry at 234 nm) from the total amount of added ADR.

To determine the kinetics of ADR release from the nanocarriers, an ADR-loaded nanocarrier suspension (3 mL, ≈1 mg/mL) was dialyzed (MWCO 14,000) against phosphate buffer (10 mM phosphate, 50 mM NaCl at pHs ranging 3.5–7.4 at 37 °C. At dialysis times of 1, 3, 5, 7, 10, and 24 h, ADR concentrations in the outside solution were determined by spectrophotometry at a wavelength of 234 nm.

#### 2.5. Cell culture

HeLa cells were grown and maintained in RPMI 1640 medium with 10% FBS and 5% penicillin-streptomycin in a humidified atmosphere with 5% CO<sub>2</sub> at 37 °C.

#### 2.6. Flow cytometry

Cells (5 × 10<sup>4</sup> cells/mL) were harvested from monolayers by a 0.25% (w/v) trypsin–0.03% (w/v) EDTA solution. After 1 mL of RPMI 1640 was added to each well of a 12-well plate, cells in 200 µL of RPMI 1640 (with or without folic acid) were seeded in each well

and were incubated for 24 h. When the cells reached 90% confluence, the medium was removed and the cells were washed twice with phosphate buffered saline (PBS, pH 7.4). The cells were then treated with ADR-loaded nanoparticles or free ADR (40 µg/mL ADR) in a humidified incubator with 5% CO<sub>2</sub> atmosphere at 37 °C. After 3 h of incubation, the medium was discarded and the cells were washed twice with 2 mL of PBS. Cells were then detached by 0.25% (w/v) trypsin–0.03% (w/v) EDTA solution and dispersed in 0.5 mL of PBS for flow cytometric measurements. Nanocarrier uptake was analyzed based on the ADR fluorescence using a FACSCalibur flow cytometer (BD Biosciences). A minimum of 1 × 10<sup>4</sup> cells was analyzed from each sample, with fluorescence intensity displayed on a four-decade log scale.

#### 2.7. Confocal image analysis

For confocal laser scanning microscopy (CLSM) studies, HeLa cells cultured in RPMI 1640 (with or without folic acid) were seeded onto 22 mm round glass coverslips, placed in a 6-well plate, and grown overnight. The medium was then removed and the cells were washed twice with PBS. Cells were treated with ADR-loaded nanoparticles or free ADR (40 µg/mL ADR) for 3 h at 37 °C and 5% CO<sub>2</sub>. Cells were washed twice with PBS and fixed with 1.5% formaldehyde. Coverslips were placed onto the glass microscope slides and sample uptake was visualized at excitation and emission wavelengths of 535 and 590 nm, respectively, by a Leica TCS SP5 Confocal System installed on an upright compound microscope (Leica, Wetzlar, Germany). Digital monochromatic images were acquired using Leica Confocal Software.

#### 2.8. Cytotoxicity assay

HeLa cells were seeded in a 96-well plate at a density of 1 × 10<sup>4</sup> cells/well in RPMI 1640 medium (with or without folic acid) containing 10% FBS at 37 °C and 5% CO<sub>2</sub>. After 24 h of culture, medium in the wells was replaced with 200 µL of fresh medium containing the ADR-loaded nanoparticles or free ADR (0.5, 5, 10, 15, 25 and 40 µg/mL ADR). Each sample with the same ADR concentration was added to six wells in the same column.

After incubation for 24 h, the medium was removed and the cells were washed three times with PBS. Twenty microliters of the combined 3-(4,5-dimethylthiazol-2-yl)-5-(3-carboxymethoxyphenyl)-2-(4-sulfophenyl)-2H-tetrazolium (MTS)/phenazine methosulfate (PMS) solution (20: 1, v/v, Cell-Titer 96® Aqueous kit) was added to each well of the 96-well assay plate containing cells in 100 µL of RPMI 1640 without phenol red. After incubation for 1 h at 37 °C in a humidified 5% CO<sub>2</sub> atmosphere, the absorbance at 490 nm in each well was recorded using a SpectraMax M5 microplate reader. The spectrophotometer was calibrated to zero absorbance using culture medium without cells. The relative cell viability compared to control wells containing cell culture medium without nanoparticles was

calculated by  $[A]_{\text{test}}/[A]_{\text{control}}$ , where  $[A]_{\text{test}}$  and  $[A]_{\text{control}}$  are the average absorbances of the test and control samples, respectively.

A cytotoxicity assay was performed without folic acid at a fixed equivalent concentration of ADR and various incubation times. HeLa cells were seeded in a 96-well plate at  $1 \times 10^4$  cells/well in RPMI 1640 medium (without folic acid) containing 10% FBS. After 24 h of culture at 37 °C and 5% CO<sub>2</sub>, ADR-loaded nanoparticles or free ADR solution were added to the wells. Medium in wells of the same column (six duplicates) was replaced with fresh medium (without folic acid) containing the ADR-loaded nanoparticles or free ADR (200  $\mu$ L, 40  $\mu$ g/mL ADR) at specific times (i.e. to yield sample incubation times of 1, 3, 5, 7, 15, and 24 h). An MTS assay was used to measure the tumor cell viability.

### 3. Results and discussion

#### 3.1. Preparation and characterization of the nanocarriers

Block copolymers containing PMAA, PGMA, and PnBMA segments were synthesized by copolymerization of the corresponding tBMA, SMA, and nBMA monomers. Synthesis was initiated by PEG macroinitiators and performed by ATRP, followed by deprotection of the PtBMA and PSMA segments [24,26,27]. The block copolymer structure is shown in Table 1. Chain lengths of the

PtBMA, PnBMA and PSMA segments were determined by <sup>1</sup>H NMR using the MPEG or PEG segment as a reference.

In preparing the macroinitiator FA-PEG-Br from OH-PEG-OH and 2-bromoisobutyl bromide (1:1 M ratio), three products may be generated: OH-PEG-Br, Br-PEG-Br, and unreacted OH-PEG-OH. After coupling the polymer mixture with folic acid, the polymer product should contain the desired macroinitiator FA-PEG-Br, and Br-PEG-Br and FA-PEG-FA. Fig. 1 shows the <sup>1</sup>H NMR spectrum of the macroinitiator mixture, which displayed a broad peak at  $\delta$  3.7 ppm attributed to PEG and characteristic peaks at  $\delta$  2.3 ppm ( $\gamma$ -CH<sub>2</sub>, glutamic acid),  $\delta$  6.6 and 7.6 ppm (aromatic protons), and  $\delta$  8.6 ppm (pteridine proton) attributed to FA. Based on the FA calibration curve, the molar percent of FA in the macroinitiator was 115 mol%. After initiation and propagation of SMA by the macroinitiator and further hydrolysis of the PSMA segment to form PGMA, the resulting polymer mixture may contain FA-PEG-*b*-PGMA, PGMA-*b*-PEG-*b*-PGMA and FA-PEG-FA.

Block copolymer-coated Fe<sub>3</sub>O<sub>4</sub> nanoparticles were prepared by alkaline coprecipitation of Fe<sup>2+</sup>/Fe<sup>3+</sup> (1:2 M ratio) in the presence of copolymers in an aqueous solution according to our previously reported procedures [24,27]. The PGMA segment of the copolymers should attach to the surface of the Fe<sub>3</sub>O<sub>4</sub> nanoparticle core, while the other segments stretch into the water based on our previous researches [24,25,27]. The size and size distribution of the nanoparticles were studied by TEM and DLS. Fe<sub>3</sub>O<sub>4</sub> nanoparticles coated

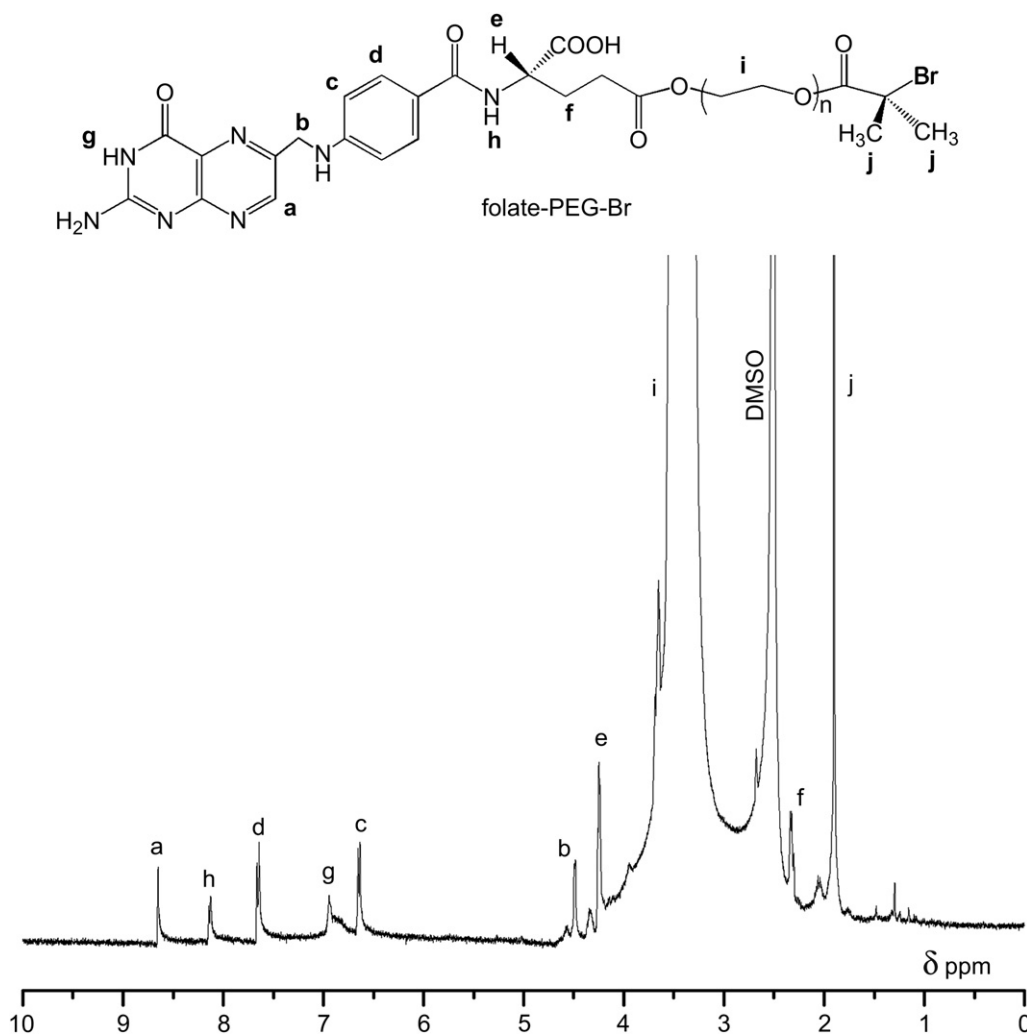


Fig. 1. <sup>1</sup>H NMR spectrum of FA-PEG-Br.



with all these block copolymers appeared similar in the TEM micrographs. Fig. 2 shows the TEM images of MPEG-*b*-PMAA<sub>18</sub>-*b*-PGMA<sub>15</sub>-Fe<sub>3</sub>O<sub>4</sub> and MPEG-*b*-P(MAA<sub>19</sub>-*co*-nBMA<sub>4</sub>)-*b*-PGMA<sub>25</sub>-Fe<sub>3</sub>O<sub>4</sub> nanoparticles. The average diameters of the core Fe<sub>3</sub>O<sub>4</sub> nanoparticles were estimated to be 7–8 nm from the images, which did not clearly depict the outside copolymers. The average hydrodynamic diameters of MPEG-*b*-PMAA<sub>18</sub>-*b*-PGMA<sub>15</sub>-Fe<sub>3</sub>O<sub>4</sub> and MPEG-*b*-P(MAA<sub>19</sub>-*co*-nBMA<sub>4</sub>)-*b*-PGMA<sub>25</sub>-Fe<sub>3</sub>O<sub>4</sub> nanoparticles dispersed in aqueous medium were 23 and 25 nm, respectively, with a similar size and narrow size distribution determined by DLS. The zeta potential of the nanoparticle dispersions was almost the same with that of distilled water (e.g., −5.7 mV for the dispersion of MPEG-*b*-P(MAA<sub>19</sub>-*co*-nBMA<sub>4</sub>)-*b*-PGMA<sub>25</sub>-Fe<sub>3</sub>O<sub>4</sub>) because of the shielding of the negatively charged carboxylate anions by the uncharged MPEG outmost shell. The high affinity of the PGMA segment for Fe<sub>3</sub>O<sub>4</sub> nanoparticles [27] and the steric shielding by the hydrophilic MPEG

outmost shell make the dispersions very stable. After more than 6 months of storage in refrigerator, no precipitation in the dispersions was observed and the hydrodynamic diameters determined by DLS remained unchanged (23–26 nm) within the error. The copolymer-coated Fe<sub>3</sub>O<sub>4</sub> nanoparticles showed superparamagnetic behavior without magnetic hysteresis according to SQUID magnetization at 300 K (Fig. 3).

### 3.2. Drug loading and release studies

ADR was loaded into the copolymer-coated Fe<sub>3</sub>O<sub>4</sub> nanoparticles containing carboxylic acid groups at neutral pH (7.4). We previously found that ADR loading into PMAA- or poly(acrylic acid) containing carriers is driven by both ionic bonding and hydrophobic interactions. The pH-responsive release kinetic profiles of loaded ADR from PMAA- or poly(acrylic acid) containing carriers are well-correlated with the pK<sub>a</sub> of polycarboxylates [24]. Since ADR binding to the nanocarriers includes ionic bonding, the release should also be responsive to the ionic strength of the release medium in addition to pH.

Fig. 4 shows the release kinetic profiles from ADR-loaded MPEG-*b*-PMAA<sub>18</sub>-*b*-PGMA<sub>15</sub>-Fe<sub>3</sub>O<sub>4</sub> nanoparticles in phosphate buffer (10 mM) without the addition of salt and with 0.9% NaCl, which mimics the physiological condition of blood. The release of the loaded ADR appeared to be responsive to the pH of the medium. Release at pH 7.4 in buffer without salt was very low, but increased significantly at lower pH values (Fig. 4a). However, release under the condition mimicking the blood environment (pH 7.4 with 0.9% NaCl) was quite high (up to 46.5% accumulation in 24 h, Fig. 4b). This would lead to severe premature release in the bloodstream if the delivery system were applied *in vivo*.

To avoid this problem, a hydrophobic moiety (PnBMA) was introduced into the PMAA-containing segments of the nanocarriers, i.e. MPEG-*b*-P(MAA<sub>19</sub>-*co*-nBMA<sub>4</sub>)-*b*-PGMA<sub>25</sub>-Fe<sub>3</sub>O<sub>4</sub> and MPEG-*b*-P(MAA<sub>17</sub>-*co*-nBMA<sub>10</sub>)-*b*-PGMA<sub>17</sub>-Fe<sub>3</sub>O<sub>4</sub>. The ADR loading capacities of these nanocarriers decreased with a decrease in the −COOH content after introduction of PnBMA (the last column of Table 2). However, the molar ratio of loaded ADR to the carboxyl groups in the carriers with PnBMA was higher than that in nanocarriers without PnBMA. The relative higher loading capacity (in the unit of moles of loaded ADR per mole of −COOH of carrier) of the carriers with PnBMA indicated that the ADR loading involved

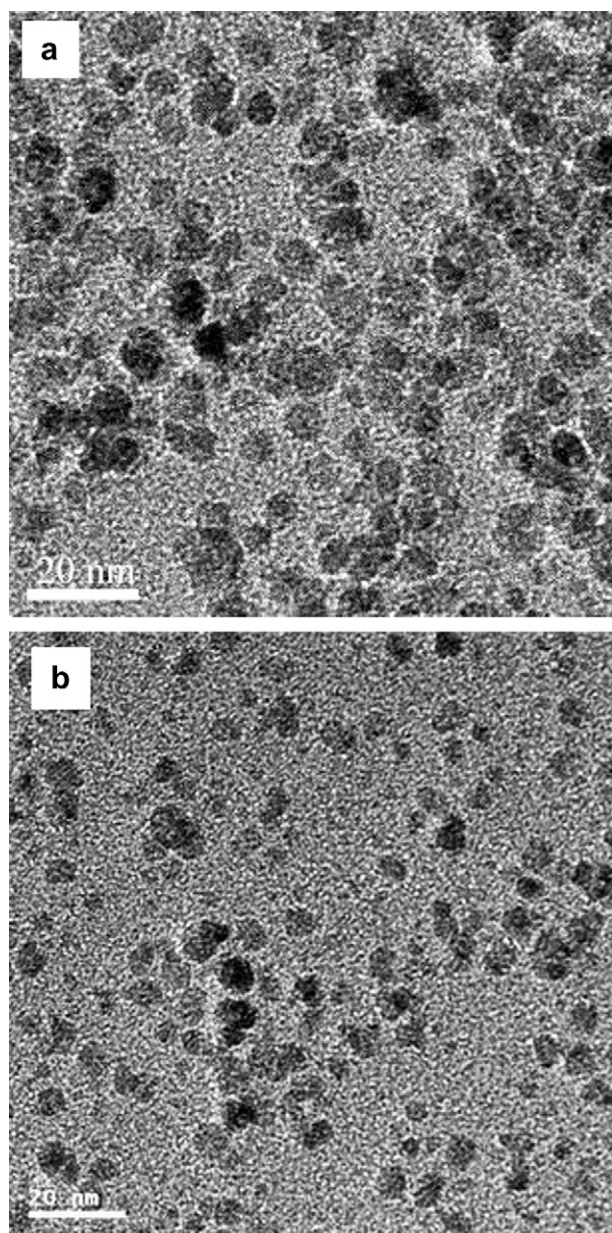


Fig. 2. TEM images of (a) MPEG-*b*-PMAA<sub>18</sub>-*b*-PGMA<sub>15</sub>-Fe<sub>3</sub>O<sub>4</sub> nanoparticles and (b) MPEG-*b*-P(MAA<sub>19</sub>-*co*-nBMA<sub>4</sub>)-*b*-PGMA<sub>25</sub>-Fe<sub>3</sub>O<sub>4</sub> nanoparticles.

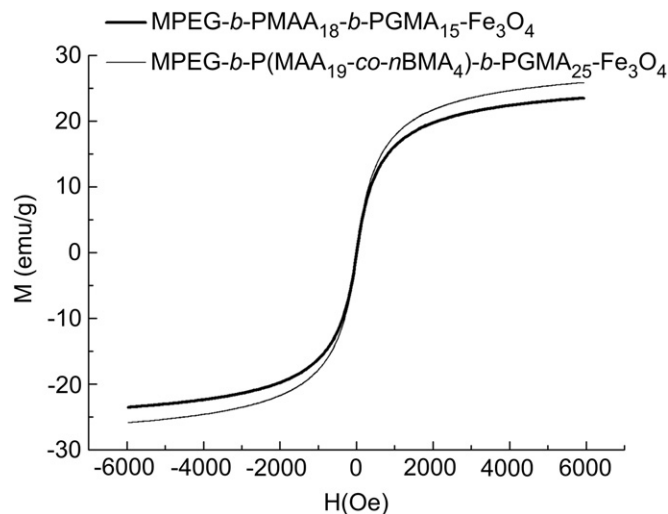
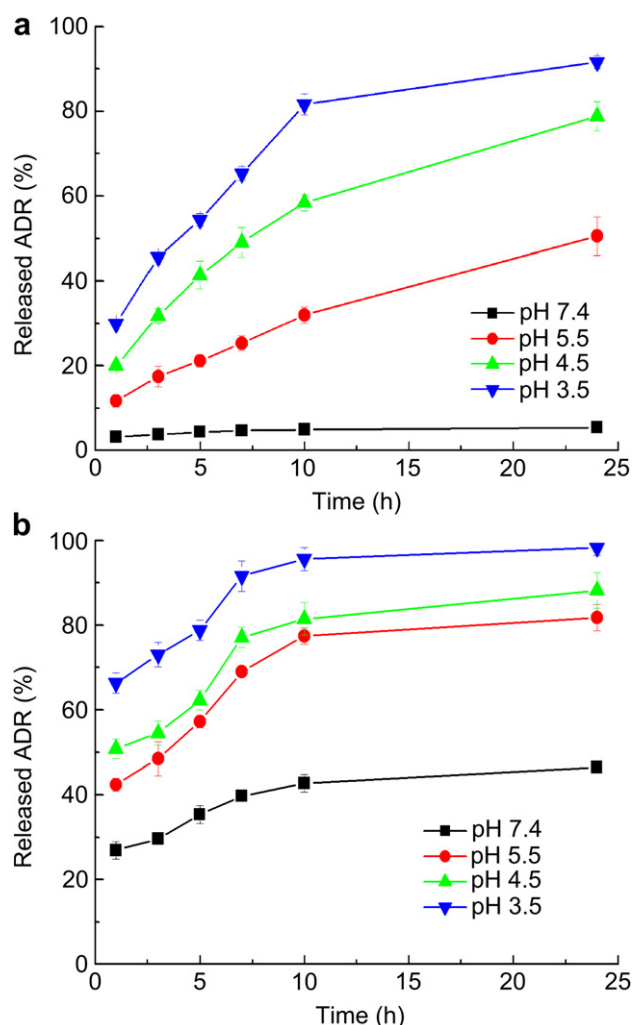


Fig. 3. SQUID magnetization of MPEG-*b*-PMAA<sub>18</sub>-*b*-PGMA<sub>15</sub>-Fe<sub>3</sub>O<sub>4</sub> and MPEG-*b*-P(MAA<sub>19</sub>-*co*-nBMA<sub>4</sub>)-*b*-PGMA<sub>25</sub>-Fe<sub>3</sub>O<sub>4</sub> nanoparticles at 300 K.



**Fig. 4.** Release of loaded ADR from MPEG-*b*-P(MAA<sub>18</sub>-*co*-nBMA<sub>15</sub>)-*b*-PGMA<sub>15</sub>-Fe<sub>3</sub>O<sub>4</sub> nanoparticles in phosphate buffer (10 mM) (a) without the addition of NaCl and (b) with 0.9% NaCl at 37 °C. Results are means  $\pm$  SD ( $n = 3$ ).

both hydrophobic interactions and ionic bonding, with cooperativity between the two.

The pH-responsive release of loaded ADR from PnBMA-containing nanocarriers under physiological-like conditions is shown in Figs. 5 and 6. Release from either nanocarrier was responsive to the pH value of the media. The release rate under bloodstream-like conditions (pH 7.4 with 0.9% NaCl) was much lower for carriers containing hydrophobic PnBMA segments (25.2% and 20.5% accumulation in 24 h from MPEG-*b*-P(MAA<sub>19</sub>-*co*-nBMA<sub>4</sub>)-*b*-PGMA<sub>25</sub>-

**Table 2**  
ADR loading capacities of the copolymer-coated Fe<sub>3</sub>O<sub>4</sub> nanoparticles.

Copolymer	-COOH content mmol/g	ADR loading capacity	
		mg/mg carrier <sup>a</sup>	mol/mol <sup>b</sup> -COOH
MPEG- <i>b</i> -PMAA <sub>18</sub> - <i>b</i> -PGMA <sub>15</sub>	1.32	0.201 $\pm$ 0.016	0.28
MPEG- <i>b</i> -P(MAA <sub>19</sub> - <i>co</i> -nBMA <sub>4</sub> )- <i>b</i> -PGMA <sub>25</sub>	0.54	0.156 $\pm$ 0.009	0.53
MPEG- <i>b</i> -P(MAA <sub>17</sub> - <i>co</i> -nBMA <sub>10</sub> )- <i>b</i> -PGMA <sub>17</sub>	0.65	0.147 $\pm$ 0.011	0.42

<sup>a</sup> Milligrams of loaded ADR per milligram of carrier. Results are means  $\pm$  SD ( $n = 3$ ).

<sup>b</sup> Moles of loaded ADR per mole of -COOH of carrier.

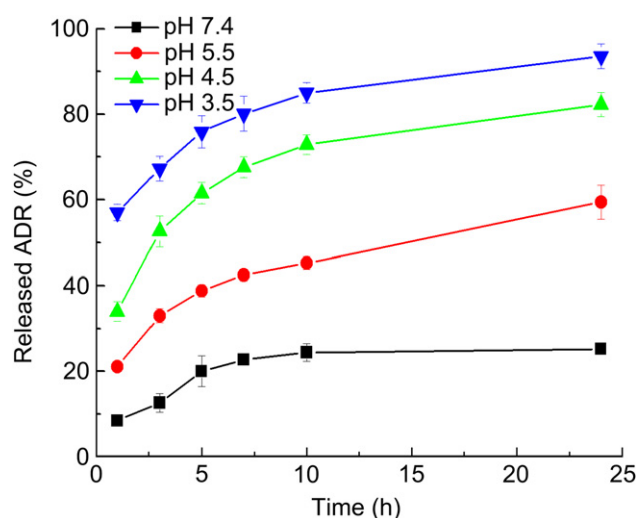


**Fig. 5.** Release of the loaded ADR from MPEG-*b*-P(MAA<sub>19</sub>-*co*-nBMA<sub>4</sub>)-*b*-PGMA<sub>25</sub>-Fe<sub>3</sub>O<sub>4</sub> nanoparticles in phosphate buffer (10 mM) with 0.9% NaCl at 37 °C. Results are means  $\pm$  SD ( $n = 3$ ).

Fe<sub>3</sub>O<sub>4</sub> and MPEG-*b*-P(MAA<sub>17</sub>-*co*-nBMA<sub>10</sub>)-*b*-PGMA<sub>17</sub>-Fe<sub>3</sub>O<sub>4</sub>, respectively, compared to 46.5% from MPEG-*b*-PMAA<sub>18</sub>-*b*-PGMA<sub>15</sub>-Fe<sub>3</sub>O<sub>4</sub>). The ADR release rate was positively correlated with the ratio of the nBMA segment to the PMAA segment in the nanocarriers. These results further indicate that ADR binding to the carriers included both ionic bonding and hydrophobic interactions. The release rate may therefore be controlled by varying the proportion of nBMA segments in the drug-loading layer of the carriers according to the hydrophobicity of the drug loaded.

### 3.3. Folate-containing nanocarrier

To conjugate folate to the surface of the pH-responsive nanocarriers, a mixture of the copolymers MPEG-*b*-P(MAA<sub>19</sub>-*co*-nBMA<sub>4</sub>)-*b*-PGMA<sub>25</sub> and folate-PEG-PGMA<sub>34</sub> (9:1 M ratio) was used to prepare the magnetic nanocarrier, i.e. MPEG-*b*-P(MAA<sub>19</sub>-*co*-nBMA<sub>4</sub>)-*b*-PGMA<sub>25</sub>/FA-PEG-GMA<sub>34</sub>-Fe<sub>3</sub>O<sub>4</sub> (denoted FA-Carrier). Flow cytometry analysis was used to compare cellular uptake of ADR-loaded MPEG-*b*-P(MAA<sub>19</sub>-*co*-nBMA<sub>4</sub>)-*b*-PGMA<sub>25</sub>/FA-PEG-GMA<sub>34</sub>-Fe<sub>3</sub>O<sub>4</sub> (denoted FA-Carrier-ADR) with those of ADR-loaded MPEG-*b*-P(MAA<sub>19</sub>-*co*-nBMA<sub>4</sub>)-*b*-PGMA<sub>25</sub>-Fe<sub>3</sub>O<sub>4</sub> (denoted Carrier-

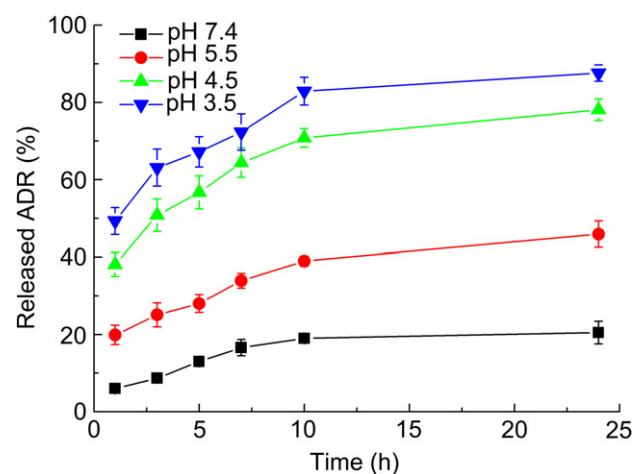


**Fig. 6.** Release of the loaded ADR from MPEG-*b*-P(MAA<sub>17</sub>-*co*-nBMA<sub>10</sub>)-*b*-PGMA<sub>17</sub>-Fe<sub>3</sub>O<sub>4</sub> nanoparticles in phosphate buffer (10 mM) with 0.9% NaCl at 37 °C. Results are means  $\pm$  SD ( $n = 3$ ).

ADR) and free ADR, using a folate receptor-expressing HeLa cell line.

FA-Carrier-ADR, Carrier-ADR, and free ADR (each with 40  $\mu\text{g}/\text{mL}$  ADR) were incubated with cells in folate-containing or folate-free culture media for 3 h. The amount of each sample internalized by the cells should be proportional to the fluorescence intensity of ADR (as a fluorescent marker). Fig. 7 shows the flow cytometry results of FA-Carrier-ADR and Carrier-ADR in the presence and absence of folate in the medium. Little difference was observed in the cellular uptake of ADR when HeLa cells were incubated with Carrier-ADR, regardless of folate addition (Fig. 7A). However, when HeLa cells were incubated with FA-Carrier-ADR, much greater cellular uptake was observed in the folate-free than in the folate-containing medium (Fig. 7B). Presumably, folate in the medium prevented FA-Carrier-ADR from transporting into HeLa cells by competitive binding to folate receptors on the cell surface, indicating that the FA-Carrier-ADR was transported into the cells by a folate receptor-mediated endocytosis process.

The flow cytometry profiles of HeLa cells incubated for 3 h with FA-Carrier-ADR, Carrier-ADR, or free ADR are shown in Fig. 8. Cells without any ADR sample treatment were used as a negative control. With the equivalent ADR concentration in each formulation (40  $\mu\text{g}/\text{mL}$  ADR) and the same incubation time, FA-Carrier-ADR displayed a higher fluorescence intensity than Carrier-ADR, verifying that the FA-Carrier-ADR was targeted to HeLa cells by folate receptor-mediated endocytosis. These results indicate that the cellular

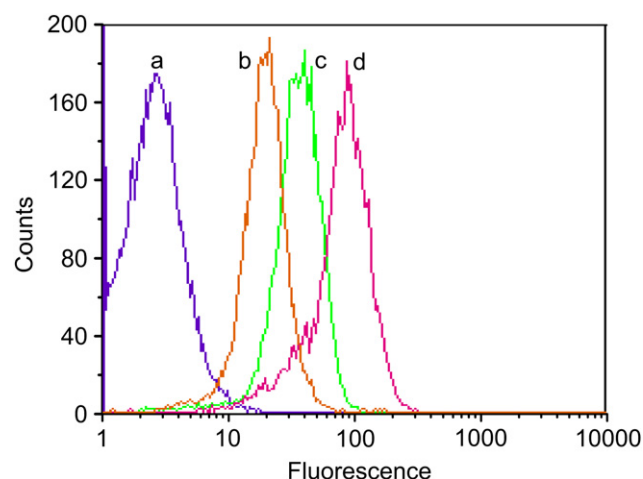


Fig. 8. Flow cytometric histogram profiles of change in fluorescence intensity when HeLa cells were exposed to (a) control, (b) Carrier-ADR, (c) FA-Carrier-ADR, or (d) free ADR in folate-free medium for 3 h.

uptake of the drug-loaded carriers is enhanced by attaching folate to their surface. The higher cellular uptake of free ADR compared to FA-Carrier-ADR or Carrier-ADR can be attributed to the faster diffusion of the small molecules than the nanoparticles in the cells in the *in vitro* assay, in which the passive targeting (the EPR effect) should not exist.

Folate receptor-mediated cellular uptake of FA-Carrier-ADR was also evaluated using CLSM analysis (Fig. 9). There was no detectable change in the fluorescence intensity of HeLa cells cultured in folate-containing or folate-free media after a 3-h incubation with Carrier-ADR (Fig. 9a and b), indicating that Carrier-ADR might be taken up by the cells through a non-specific endocytosis mechanism. In contrast, more fluorescently marked cells were clearly visualized in the folate-free medium than in the folate-containing medium after incubation with FA-Carrier-ADR (Fig. 9c and d), consistent with our flow cytometry results. The fluorescence intensity of HeLa cells cultured with FA-Carrier-ADR in folate-free medium (Fig. 9d) was much higher than that of cells cultured with Carrier-ADR (Fig. 9b), and was similar to that of cells cultured with free ADR (Fig. 9f). FA-Carrier-ADR could therefore be targeted to HeLa cells by a folate receptor-mediated endocytosis process. The rate of the endocytosis was comparable to that of the diffusion process of free ADR, but much faster than that of the non-specific endocytosis process of Carrier-ADR. All of these studies reconfirmed that the cellular uptake of drug-loaded carriers could be significantly accelerated by the surface-conjugation of folate.

### 3.4. Cytotoxicity analysis

Flow cytometry and confocal microscopy analyses showed that FA-Carrier-ADR could be targeted and endocytosed into HeLa cells by a fast folate receptor-mediated endocytosis process. Upon uptake, the loaded ADR would be released in endosomes and lysosomes due to the acidic conditions, and thereby inhibit cancer cell growth. Fig. 10a shows the growth inhibition of HeLa cells by Carrier-ADR, FA-Carrier-ADR, and free ADR in folate-containing medium. Carrier-ADR and FA-Carrier-ADR exhibited similar cellular growth inhibition levels that were lower than that of free ADR. The overexpressed surface folate receptors on the cancer cells should have been presaturated with free folate in the medium, thereby blocking folate receptor-mediated endocytosis. FA-Carrier-ADR should only be taken up through a slow non-specific endocytosis mechanism like Carrier-ADR.

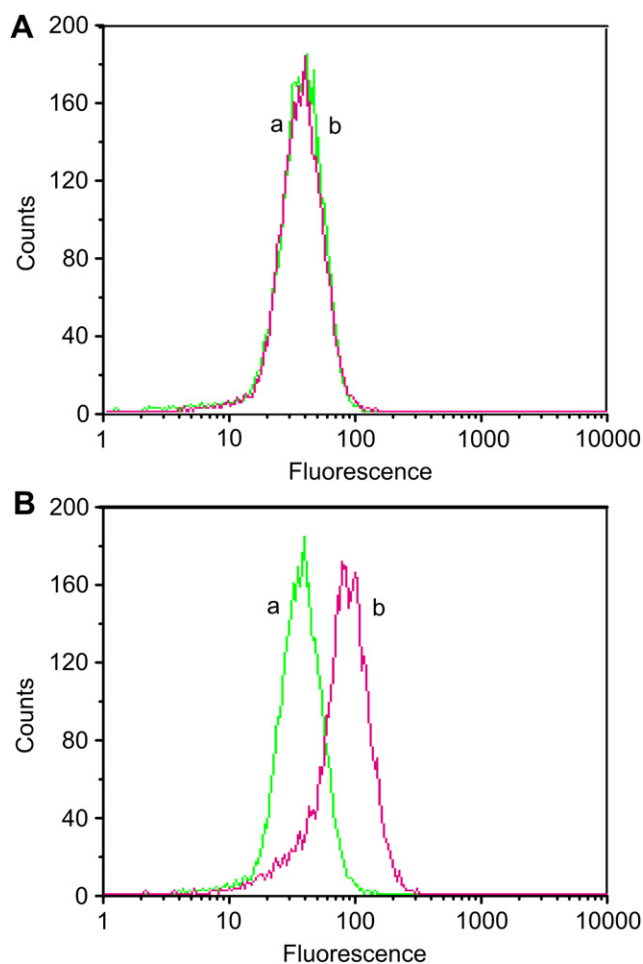
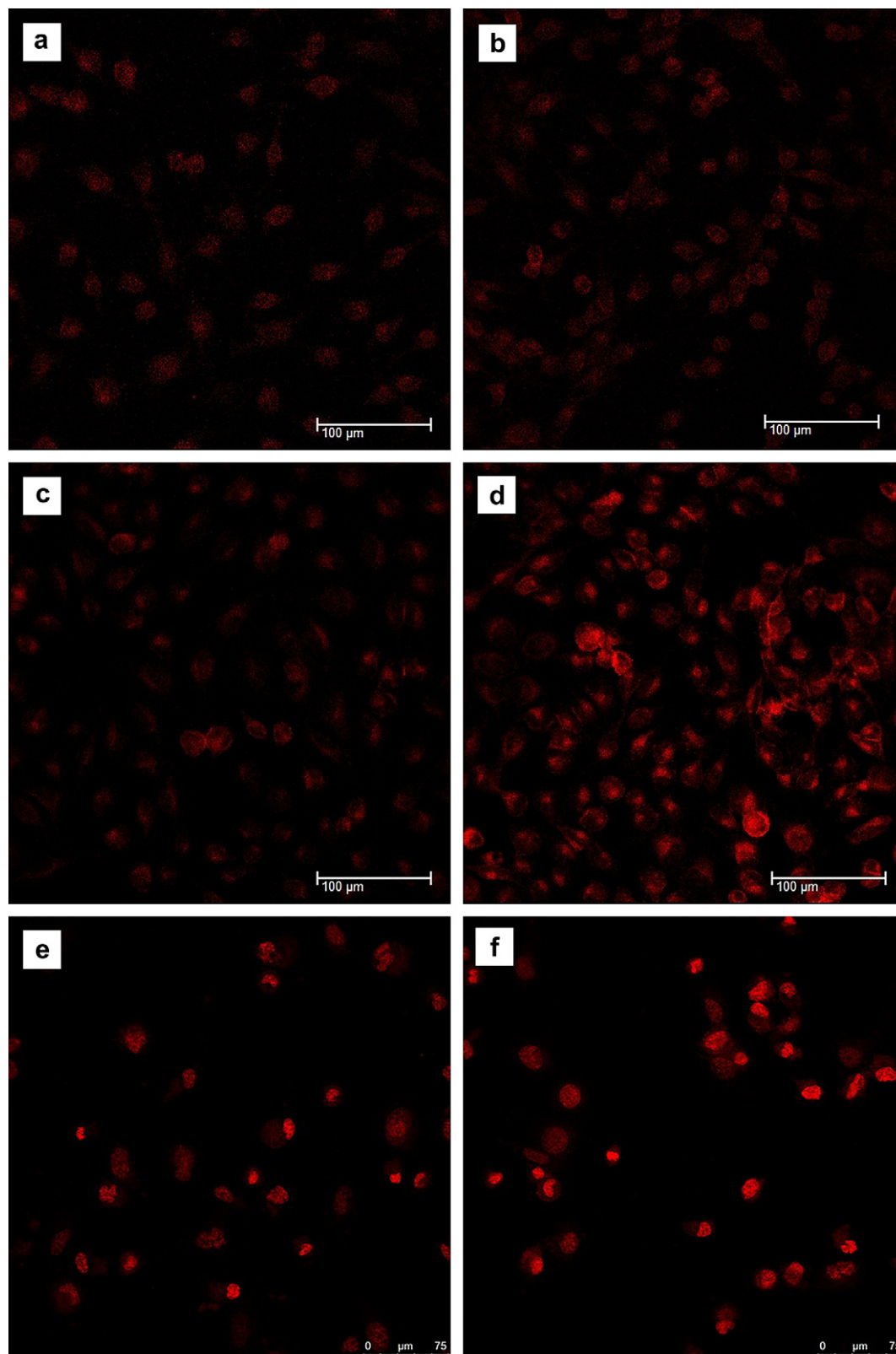


Fig. 7. Flow cytometry results of (A) Carrier-ADR and (B) FA-Carrier-ADR in (a) folate-containing or (b) folate-free media.





**Fig. 9.** Confocal microscopic images of HeLa cells incubated with (a, b) Carrier-ADR, (c, d) FA-Carrier-ADR, or (e, f) free ADR in (a, c, e) folate-containing or (b, d, f) folate-free media.

Both of the ADR-loaded carriers showed lower cytotoxicities than free ADR, perhaps due to the slower endocytosis process of ADR-loaded carriers compared to the diffusion process of free ADR. In contrast, FA-Carrier-ADR exhibited a higher cytotoxicity than

Carrier-ADR, but similar cytotoxicity with free ADR in the folate-free medium (Fig. 10b). This can be attributed to the higher uptake of FA-Carrier-ADR than Carrier-ADR by HeLa cells, followed by the ADR release after entering into the cells.



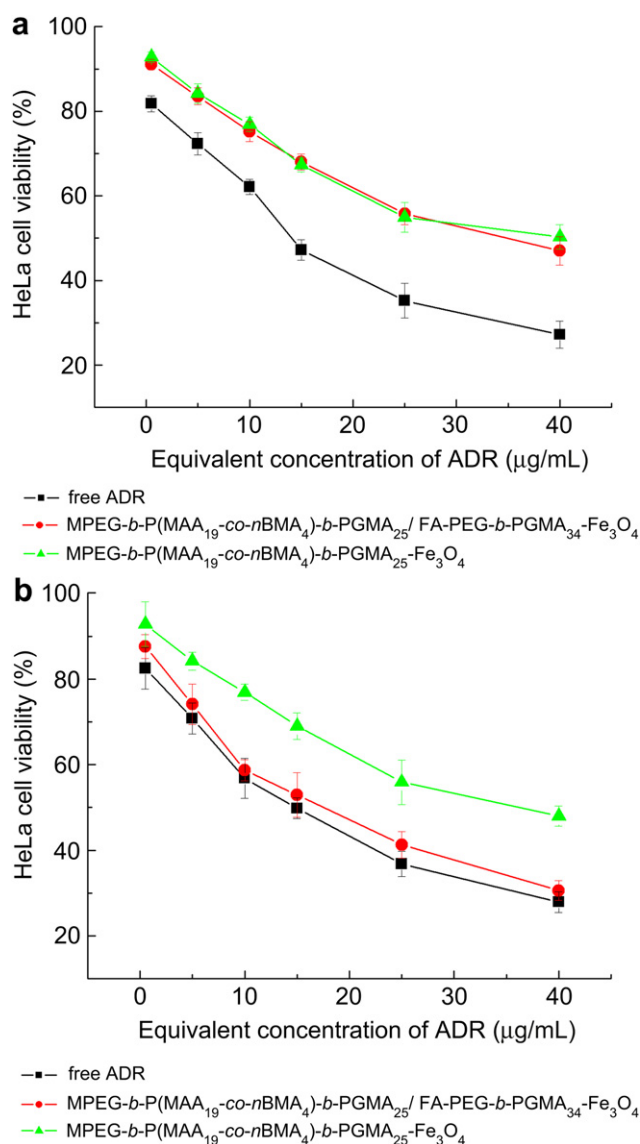


**Fig. 10.** Viability of HeLa cells incubated with Carrier-ADR, FA-Carrier-ADR, or free ADR at different concentrations in (a) folate-containing medium and (b) folate-free medium.

Considering that the cytotoxicity of intracellular environment-sensitive drug carriers tends to be time-dependent [29,30,31], we also incubated HeLa cells in folate-free medium containing FA-Carrier-ADR, Carrier-ADR, or free ADR (all 40  $\mu\text{g/mL}$  ADR) with exposure times of 1, 3, 5, 7, 15 and 24 h. The cytotoxicity of FA-Carrier-ADR was similar to that of Carrier-ADR, but much lower than that of free ADR before 5 h. With longer incubation times, the cytotoxicity of FA-Carrier-ADR approached that of free ADR and gradually became higher than that of Carrier-ADR (Fig. 11). The fact that FA-Carrier-ADR could be targeted and endocytosed into HeLa cells by a fast folate receptor-mediated endocytosis process was shown in our flow cytometry and confocal microscopy analyses. However, endocytosed FA-Carrier-ADR only released a small quantity of the loaded ADR and exhibited a much lower cytotoxicity than free ADR at short exposure times. FA-Carrier-ADR showed a gradually increasing cytotoxicity with the increase in ADR release, achieving a similar cytotoxicity to free ADR. These results confirm the time-dependent growth inhibitory mechanism and folate-mediated cancer cell targeting properties of FA-Carrier-ADR.

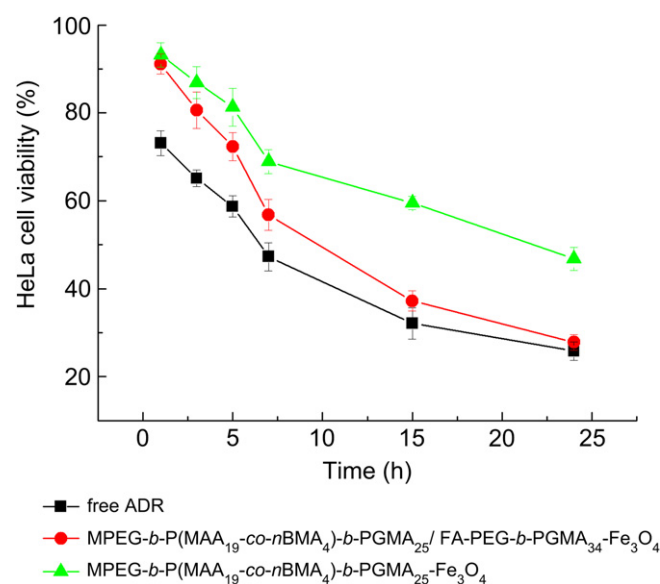


**Fig. 11.** Time-dependent growth inhibitory effects of Carrier-ADR, FA-Carrier-ADR, and free ADR in folate-free medium.

#### 4. Conclusions

Nanoparticles with an  $\text{Fe}_3\text{O}_4$  core and MPEG-*b*-P(MAA<sub>19</sub>-*co*-nBMA<sub>4</sub>)-*b*-PGMA<sub>25</sub>/FA-PEG-PGMA<sub>34</sub> shell were prepared as a tumor-targeted drug delivery system. As a model drug, ADR was loaded into the carboxyl-containing inner shell composed of P(MAA-*co*-nBMA) by a combination of ionic bonding and hydrophobic interactions at pH 7.4. The release of the loaded drugs from the nanocarriers was pH-responsive. At endosomal/lysosomal acidic pH (<5.5), the protonation of the polycarboxylate anions of PMAA broke the ionic bond between the carrier and ADR, leading to ADR release. This is because the hydrophobic interaction alone is weak due to the relatively hydrophilic nature of the nanocarrier. Cellular uptake and cytotoxicity studies showed that FA-Carrier-ADR displayed a greater cellular uptake than Carrier-ADR. FA-Carrier-ADR was taken up by a folate receptor-mediated endocytosis process, resulting in enhanced cytotoxicity against HeLa cells. These results indicate that the MPEG-*b*-P(MAA-*co*-nBMA)-*b*-PGMA/FA-PEG-PGMA- $\text{Fe}_3\text{O}_4$  nanoparticles could be used as a potential folate-mediated, pH-responsive drug-releasing nanocarrier for anticancer drug delivery. The promising results encourage us to perform further *in vivo* delivery in an animal model in the future.

#### Acknowledgements

This work was supported by the National Natural Science Foundation of China (Grant No. 20974052), the National Key Technologies R & D Program for New Drugs of China (Grant No. 2009ZX09301-002), and the Natural Science Foundation of Tianjin Municipality (Grant No. 09JCZDJC22900).

#### Appendix

Figure with essential color discrimination. Figs. 4–11 in this article is difficult to interpret in black and white. The full color images can be found in the on-line version, at [doi:10.1016/j.biomaterials.2010.09.077](https://doi.org/10.1016/j.biomaterials.2010.09.077).

## References

- [1] Alemdaroglu FE, Alemdaroglu NC, Langguth P, Herrmann A. DNA block copolymer micelles – a combinatorial tool for cancer nanotechnology. *Adv Mater* 2008;20:899–902.
- [2] Misra RD. Magnetic nanoparticle carrier for targeted drug delivery: perspective, outlook and design. *Mater Sci Tech* 2008;24:1011–9.
- [3] Sun C, Lee Jerry SH, Zhang M. Magnetic nanoparticles in MR imaging and drug delivery. *Adv Drug Deliv Rev* 2008;60:1252–65.
- [4] Doshi N, Mitragotri S. Designer biomaterials for nanomedicine. *Adv Funct Mater* 2009;19:3843–54.
- [5] Farrell D, Alper J, Ptak K, Panaro NJ, Grodzinski P, Barker AD. Recent advances from the national cancer institute alliance for nanotechnology in cancer. *ACS Nano* 2010;2:589–94.
- [6] Maeda H, Matsumura Y. Tumouritropic and lymphotropic principles of macromolecular drugs. *Crit Rev Ther Drug Carrier Syst* 1989;6:193–210.
- [7] Ohtsuka N, Konno T, Miyauchi Y, Maeda H. Anticancer effects of arterial administration of the anticancer agent SMANCS with lipiodol on metastatic lymph nodes. *Cancer* 1987;59:1560–5.
- [8] Wagner E. Programmed drug delivery: nanosystems for tumor targeting. *Expert Opin Biol Ther* 2007;7:587–93.
- [9] Weitman SD, Lark RH, Coney LR, Fort DW, Frasca V, Zurawski VR, et al. Distribution of the folate receptor GP38 in normal and malignant cell lines and tissues. *Cancer Res* 1992;52:3396–401.
- [10] Campbell IG, Jones TA, Foulkes WD, Trowsdale J. Folate-binding protein is a marker for ovarian cancer. *Cancer Res* 1991;51:5329–38.
- [11] Stella B, Arpicco S, Peracchia MT, Desmaele D, Hoebeke J, Renoir M, et al. Design of folic acid-conjugated nanoparticles for drug targeting. *J Pharm Sci* 2000;89:1452–64.
- [12] Bae Y, Jang WD, Nishiyama N, Fukushima S, Kataoka K. Multifunctional polymeric micelles with folate-mediated cancer cell targeting and pH-triggered drug releasing properties for active intracellular drug delivery. *Mol Biosyst* 2005;1:242–50.
- [13] Kamaly N, Kalber T, Thanou M, Bell JD, Miller AD. Folate receptor targeted bimodal liposomes for tumor magnetic resonance imaging. *Bioconj Chem* 2009;20:648–55.
- [14] Prabakaran M, Grailer JJ, Pilla S, Steeber DA, Gong S. Folate-conjugated amphiphilic hyperbranched block copolymers based on Boltorn H40, poly(L-lactide) and poly(ethylene glycol) for tumor-targeted drug delivery. *Biomaterials* 2009;30:3009–19.
- [15] Ganta S, Devalapally H, Shahiwal A, Amiji M. A review of stimuli-responsive nanocarriers for drug and gene delivery. *J Control Release* 2008;126:187–204.
- [16] Torchilin V. Multifunctional and stimuli-sensitive pharmaceutical nanocarriers. *Eur J Pharm Biopharm* 2009;71:431–44.
- [17] Motornov M, Roiter Y, Tokarev I, Minko S. Stimuli-responsive nanoparticles, nanogels and capsules for integrated multifunctional intelligent systems. *Prog Polym Sci* 2010;35:174–211.
- [18] Bae Y, Fukushima S, Harada A, Kataoka K. Design of environment-sensitive supramolecular assemblies for intracellular drug delivery: polymeric micelles that are responsive to intracellular pH change. *Angew Chem Int Ed* 2003;42:4640–3.
- [19] Bae Y, Nishiyama N, Fukushima S, Koyama H, Matsumura Y, Kataoka K. Preparation and biological characterization of polymeric micelle drug carriers with intracellular pH-triggered drug release property: tumor permeability, controlled subcellular drug distribution, and enhanced in vivo antitumor efficacy. *Bioconj Chem* 2005;16:122–30.
- [20] Lee ES, Na K, Bae YH. Polymeric micelle for tumor pH and folate-mediated targeting. *J Control Release* 2003;91:103–13.
- [21] Kim D, Lee ES, Taek K, Gao ZG, Bae YH. Doxorubicin-loaded polymeric micelle overcomes multidrug resistance of cancer by double-targeting folate receptor and early endosomal pH. *Small* 2008;4:2043–50.
- [22] Lee Y, Fukushima S, Bae Y, Hiki S, Ishii T, Kataoka K. A protein nanocarrier from charge-conversion polymer in response to endosomal pH. *J Am Chem Soc* 2007;129:5362–3.
- [23] Oishi M, Nagatsugi F, Sasaki S, Nagasaki Y, Kataoka K. Smart polyion complex micelles for targeted intracellular delivery of PEGylated antisense oligonucleotides containing acid-labile linkages. *ChemBioChem* 2005;6:718–25.
- [24] Guo M, Yan Y, Zhang H, Yan H, Cao Y, Liu K, et al. Magnetic and pH-responsive nanocarriers with multilayer core-shell architecture for anticancer drug delivery. *J Mater Chem* 2008;18:5104–12.
- [25] Guo M, Yan Y, Liu X, Yan H, Liu K, Zhang H, et al. Multilayer nanoparticles with a magnetite core and a polycation inner shell as pH-responsive carriers for drug delivery. *Nanoscale* 2010;2:434–41.
- [26] Zhen Y, Wan S, Liu Y, Yan H, Shi R, Wang C. Atom transfer radical polymerization of solketal acrylate using cyclohexanone as the solvent. *Macromol Chem Phys* 2005;206:607–12.
- [27] Wan S, Zheng Y, Liu Y, Yan H, Liu K. Fe<sub>3</sub>O<sub>4</sub> nanoparticles coated with homopolymers of glycerol mono(meth)acrylate and their block copolymers. *J Mater Chem* 2005;15:3424–5430.
- [28] Gupta AK, Curtis ASG. Lactoferrin and ceruloplasmin derivatized superparamagnetic iron oxide nanoparticles for targeting cell surface receptors. *Biomaterials* 2004;25:3029–40.
- [29] D'souza AJM, Topp EM. Release from polymeric prodrugs: linkages and their degradation. *J Pharm Sci* 2004;93:1962–79.
- [30] Jensen KD, Nori A, Tijerina M, Kopeckova P, Kopecek J. Cytoplasmic delivery and nuclear targeting of synthetic macromolecules. *J Control Release* 2003;87:89–105.
- [31] Nishiyama N, Kato Y, Sugiyama Y, Kataoka K. Cisplatin-loaded polymer-metal complex micelle with time-modulated decaying property as a novel drug delivery system. *Pharm Res* 2001;18:1035–41.